Spreading of giant vesicles on moderately adhesive substrates by fingering: A reflection interference contrast microscopy study

Toni J. Feder,[1] Gilberto Weissmüller,[1] Boštjan Žekš,[2] and Erich Sackmann[1]
[1]*Biophysics Group E22, Technical University of Munich, D-85748 Garching, Germany*
[2]*Institute of Biophysics, University of Ljubljana, SLO-61105 Ljubljana, Lipičeva 2, Slovenia*
(Received 15 July 1994)

The spreading of giant vesicles of neutral phospholipids on avidin-covered solid substrates is studied by reflection interference contrast microscopy. Contact formation, bilayer-substrate separation distances, and edge profiles are evaluated. The spreading occurs in two steps: advancement of lobes of average thickness ≈ 70 nm by fingering, sometimes followed by thinning to $\approx 30 \pm 10$ nm, determined by interfacial forces, and resulting in a pancakelike shape. The average advancement speed of the fingers appears constant at early times (≈ 0.2 μm/s) and slows down at a later stage. Locally, the bilayer advances stepwise owing to discontinuous water expulsion. The spreading is impeded by pinning centers resulting in fjord formation. The vesicle spreading is tentatively interpreted in terms of the classical theory of viscous fingering.

PACS number(s): 81.15.Lm, 68.10.Gw

I. INTRODUCTION

The spreading of simple pure liquids and polymer solutions on solids has gained much attention in recent years [1–4], motivated mainly by the important role wetting phenomena play in technical processes. Wetting phenomena involve interesting and rich physics, yielding important insights into interfacial interactions, hydrodynamic instabilities, and viscous fingering [5,6]. Despite its biological importance (for the formation of fluid films on the eyeball, for example), wetting in biology has gained much less attention. One important and fascinating example is the spreading of cells on surfaces, e.g., during cell locomotion [7]. The formation of pseudopodia, for example, may be at least partially determined by viscous instability.

We have investigated the adhesion of closed vesicles to solids in the interaction limit where vesicles with excess surface area spread on the surface but do not burst [8]. We are concerned primarily with nonspecific interactions of neutral phospholipid membranes on avidin-coated surfaces. The adhesion energy is such that vesicles adhere strongly, and chains of contiguous giant vesicles, which provide a lipid source, spread, forming fingerlike patterns on the surface. Both the vesicle-surface contact dynamics and the three-dimensional shape of the fingers are reconstructed using the sensitive technique of reflection interference contrast microscopy (RICM), which allows direct measurement of the thicknesses of spreading films. The two models we consider, one an analogy to viscous fingering, and the other based on adhesion-driven water expulsion, cannot fully explain our observations.

II. MATERIALS AND METHODS

A. Vesicle preparation

Vesicles were prepared by swelling in an electric field as described in [9]. 5–10 mg/ml phospholipid [*L*-α-dimyristoyl phosphatidylcholine (DMPC) or *L*-α-phosphatidylcholine from egg yolk (EggPC); Sigma, St. Louis, MO] was dissolved in a 2:1 solution of chloroform:methanol (Merck, Darmstadt, Germany). 40–50 μl of the lipid stock solution was spread on electrodes composed of indium tin oxide coated glass (ITO; Balzers, Lichtenstein). The solvent was allowed to evaporate in a vacuum chamber for at least two hours. The coated electrodes were then installed in a home-built chamber, the wells separating two opposing electrodes were filled with Millipore water, and a 10 Hz, 18 V/cm electric field was applied for 1–2 h at 40 °C. Vesicles were observed first in phase contrast microscopy to ascertain that successful swelling had occurred. A typical sample contains vesicles of a wide range of sizes (with some larger than 150 μm in diameter) and shapes, some with internal vesicles, and of various lamellarity.

B. Substrate preparation

Coverglasses and ITO electrode plates were cleaned by 15 min ultrasonification in a 2% solution of Hellmanex II (Hellma, Müllheim, Germany), and then by an extremely thorough rinsing (approximately 20 times) in Milli-Q water (Millipore, Molsheim, France).

Coverglasses were coated with a ≈ 55 nm layer of magnesium fluoride (MgF_2; Johnson Matthey, Karlsruhe, Germany) by vacuum deposition at 10^{-6} atm, 380 °C substrate temperature, and 3 nm/s deposition rate.

The MgF_2 coated glass was mounted with silicon grease onto a Teflon holder embedded in a copper chamber with channels for temperature control by water flow and then mounted on the microscope for imaging. At 30 °C, the temperature was above the lipid transition temperature for all experiments discussed here. 0.125 mg/ml avidin (Sigma, St. Louis, MO) in buffer (10 m*M* hepes [*N*-(2-hydroxyethyl) piperazine-*N*′-(2-ethanesulfonic acid)] *p*H 7.5) was incubated for one hour to coat the coverglass surface with a ≈ 2 nm layer of protein. The buffer was then exchanged, and after 15 min, rinsed

again before vesicles in suspension were added. Buffer was then added to fill the chamber, and the osmotic gradient also ensured that the vesicles were flaccid.

C. Reflection interference contrast microscopy

We use the sensitive technique of reflection interference contrast microscopy (RICM). The method and the particular adapted Zeiss microscope (Neofluar 63X/1.25NA Antiflex objective lens) as well as the video image processing we use (IMAGE; Wayne Rasband, National Institutes of Health; public domain) have been described previously [7,10]. The main feature of the technique is that it isolates and exploits thin film interference, giving nanometer vertical resolution. The interference pattern resulting from light reflected from the membrane and substrate is used to calculate thicknesses and absolute heights above the surface. Observation of temporal and spatial variations in the contact area and distance from the substrate allows for studies of the dynamics of adhesion. In the approximation of normal incidence, the intensity is related to the height above the surface by

$$I[s(x)]=I_1+I_2+2\sqrt{I_1 I_2}\cos[2ks(x)-\delta_1+\delta_2]\,, \qquad (1)$$

where $k=2\pi/\lambda$ is the wave number of the light ($\lambda=546.1$ nm), and I_i,δ_i are the intensity and corresponding phase shift of the light reflected from the ith surface. The term in brackets represents the total phase shift due to the optical path difference. This relation is inverted to express height in terms of intensity

$$s(x)=\frac{1}{4\pi n}\left[\arccos\left[\frac{2I(x)-(I_{\max}+I_{\min})}{I_{\max}-I_{\min}}\right]+\delta_1-\delta_2\right]\,, \qquad (2)$$

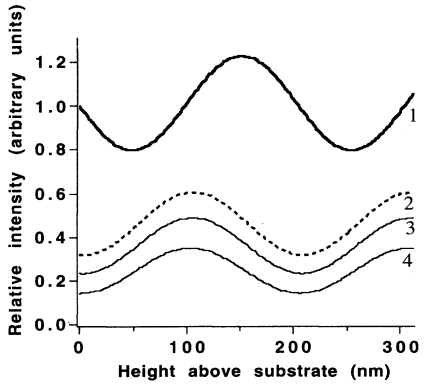

FIG. 1. Relative intensity of the interference pattern formed by light reflected from the membrane and the substrate surfaces, plotted as a function of the membrane-substrate separation. The curves shown were calculated from Eq. (2) for a phospholipid bilayer in water a distance s above a glass substrate with successive cumulative coatings: (1) glass; (2) glass coated with a 60 nm layer of MgF_2 (dashed curve); (3) 2 nm protein layer; (4) 4 nm phospholipid membrane. The MgF_2 shifts the phase by $\lambda/4$, making the adhering membrane ($s=0$) easily visible. The protein and membrane layers decrease the intensity, but do not significantly affect the phase.

where n is the index of refraction of the medium (buffer; $n=1.33$), and I_1,I_2 are expressed here in terms of the measurable quantities $I_{\min}$ and $I_{\max}$.

Because the index of refraction of glass (1.532) and that of phospholipid membrane (1.486) are similar, a membrane adhering directly to the glass, or to protein-coated glass ($n\approx 1.55$), is not well distinguished from the background. We therefore coat coverglasses with a ≈ 50 nm layer (corresponding to $\lambda/8$ optical path length) of the dielectric MgF_2 ($n=1.386$). As shown in Fig. 1, this shifts the phase such that the reflected intensity at zero separation is a minimum. The MgF_2 layer also enhances the contrast [10].

III. RESULTS

We observe a variety of forms and dynamics during vesicle adhesion, determined by the initial conditions, i.e., vesicle shape and lamellarity, osmolarity, and surface roughness. Despite the array and complexity, several generally applicable statements can be made.

(i) Fingering behavior typically originates at a "clump" of interconnected vesicles that share one unilamellar membrane envelope and have a shared interior (Fig. 2). The clump provides a source of lipids during spreading, which proceeds away from the source clump.

(ii) In the intermediate regime of moderately strong adhesion, the membrane spreads on the surface, retaining its original topology, but flattening and developing fractal-like fingers. If the attraction is too strong, vesicles burst (Fig. 3); if it is too weak, no adhesion is observed.

An example of fingering is shown in Fig. 4(a). The shape imaged is the region of adhesion of the proximal bilayer. The slight lateral intensity variations in the central region of the lobe indicate undulations of the upper, nonadhered, membrane. Along the contour of the adhering vesicle interference fringes are visible. The lobe divides into fingers separated by "fjords". At the spreading fronts, the contour is corrugated, exhibiting small precursor wetting tips [Fig. 4(a), arrows]. The spreading is characterized by very local abrupt starts and stops, and

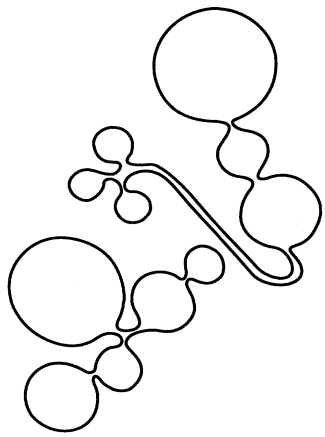

FIG. 2. Diagram of vesicle clumps.

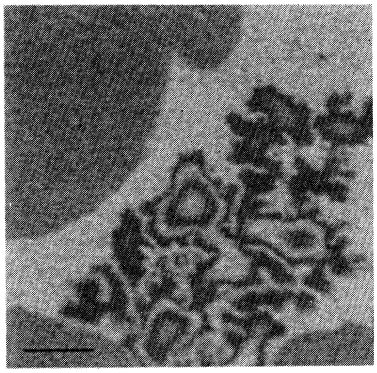

FIG. 3. DMPC vesicles were introduced to a bare MgF_2 surface. Most vesicles burst, forming large regular patches, from which the bilayer thickness can be determined. The central region of this figure shows fingering of closed vesicles on the same surface. The scale of fingers is smaller than on avidin (Fig. 4). The bar is 5 μm long.

proceeds with average speeds of 0.05–2 μm/s, generally following the directions anticipated by the precursor tips or filling in the "bays" between tips. The speed of the actual jumps is generally faster, and can be as high as ≈ 10 μm/s. The jump length is of the order of 1 μm. Figure 4(c) shows diagrams of the spreading front for spreading in four directions of the finger in Fig. 4(a). The spreading in different directions is not correlated.

In Fig. 5 we show a plot of speed versus time of measurement. The speeds represent the average of several measurements at different positions. The motion is in fact very abrupt, and changes direction frequently. In Fig. 5 the speeds are averaged, with the latent periods included. Jumps are less frequent and shorter at later times, and the speed during a jump is usually, but not necessarily, lower than at early times. Although the motion is always abrupt, and there is always a rather wide range of speeds, the rate of advancement decreases with time. The lobes can spread to quite extended lengths, dividing into progressively more branches. In Fig. 4, for example, fingers ultimately spread as far as 200 μm. Spreading ceases altogether when the lipid source (clump) is depleted.

In some cases, the upper membrane approaches the adhered one. Starting from the clump origin, the upper membrane clings progressively to the lower one, proceeding outward towards the tips. This close contact, or thinning, between the two bilayers can occur only if they are close enough for van der Waals interactions to be significant, and may perhaps be initiated by motion of the clump, either thermal or by tension arising due to the spreading lobes. The adhesion of the upper membrane to the lower is easily identifiable in RICM by the reduced intensity (Fig. 6). The undulations of the distal membrane cease. Existing fjords mapped out by the lower, already adhered membrane and defining the individual fingers, are respected. The pressure of the approaching membrane occasionally causes depinning, and the corresponding rapid disappearance of a fjord. The lobe continues to thin, with the clinging upper membrane contained by the remaining borders (Fig. 6).

The cross-sectional profile of the spreading vesicle can

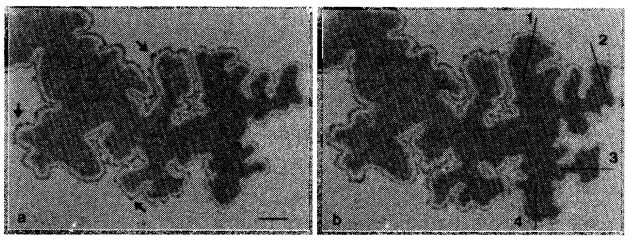

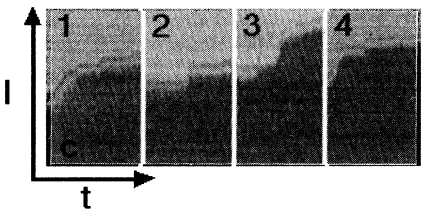

FIG. 4. EggPC vesicle spreading on an avidin surface. (a) and (b) are the first and last images in a 64 image sequence, 36 s apart. The higher intensity in the upper left corner is due to reflections from the clump, located just outside the field of view. (c) shows the advancement of the front of the fingers in the directions marked in (b). Each speed profile is a composite of the intensity profiles for the 64 frame sequence, with time proceeding to the right (t), and the position of the moving front plotted on the vertical axis (l). The average speed is then obtained from the slope (the speeds during the fast spurts, as opposed to the average overall speed, are given in parentheses): 1: 90 nm/s (310 nm/s); 2: 40 nm/s (720 nm/s); 3: 110 nm/s (850 nm/s); 4: 70 nm/s (390 nm/s). (a) and (b) are reduced in size relative to (c). The bar is 5 μm long.

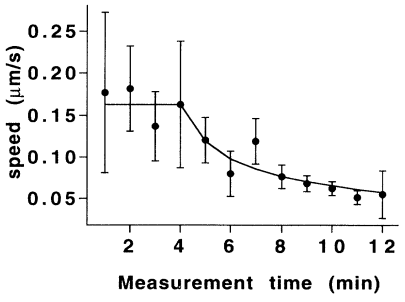

FIG. 5. Speed versus measurement time for the spreading vesicle of Fig. 4. Although the motion is abrupt, and the range of values is wide, especially during faster spreading, the velocity clearly decreases at later times. Error bars represent the range of values measured (approximately 3 measurements per time point). The curve represents a fit to the viscous fingering model in the Appendix [cf. Eq. (A5)]. A constant speed is expected at early times, and the later points ($t > 4$ min) are fit to $v(t) = A/\sqrt{t - t_0}$, where $A^2 = W(r-h)/\eta \approx 0.03$ μm^2/s. This gives a low value for the adhesion energy, $W \approx 10^{-9}$ J/m^2.

FIG. 6. EggPC vesicle spreading on avidin surface. The dark regions in this figure indicate the adhesion of the upper membrane to the lower, already adhered one. This adhesion mostly follows the existing fjords, but sometimes induces the disappearance of one, as seen in this series of images (arrow) ($\Delta t_{AB}=0.08$ s, $\Delta t_{BC}=1.8$ s). The bar is 5 μm long.

be constructed from Eq. (2). An example is shown in Fig. 7. The inverse cosine in the relationship means that each intensity corresponds to more than one separation distance (Fig. 1), leading to some ambiguity in determining the correct cross-sectional form. However, because in many cases the maximum intensity (corresponding to ≈ 100 nm, cf. Fig. 1) is not attained, the ambiguity is eliminated. Based on this argument, the thicker form [Fig. 7(b)] can be ruled out, leaving the flatter form, with its bulging, upwardly protruding edges as the only possibility [Fig. 7(a)]. The flickering upper membrane is separated by about 70 nm from the adhered one.

A reconstruction of the membrane cross section for the case of thinning, with close approach of the upper membrane to the lower, is depicted in Fig. 8. Again, while in this particular case two forms are possible, the form in Fig. 8(b) can often be eliminated by the intensity maximum observed. The bright halo at the border between the adhered (dark) and the still flickering (brighter) regions of the upper membrane (cf. Fig. 6), may be an artifact due to diffraction at the abrupt change in thickness of the steeply bent membrane at this interface, rather than an actual reflection of the height above the surface. There should be a tension exerted, pulling the distal part down towards the adhered membrane; we have sketched a curve in Fig. 8(a) to show this possibility.

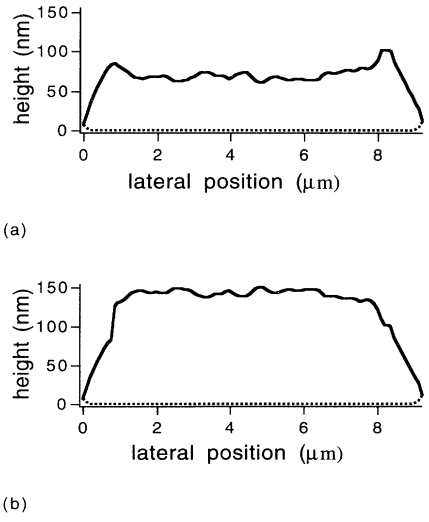

FIG. 7. Cross-sectional profiles of a spreading finger. Two forms were calculated from the intensity profile using Eq. (2). The form in (b) is possible only if the intensity maximum measured reaches the first peak in Fig. 1 (≈ 100 nm). Since this is often not the case, (a), with its bulging edge, is the more probable edge contour for spreading vesicles such as in Fig. 4.

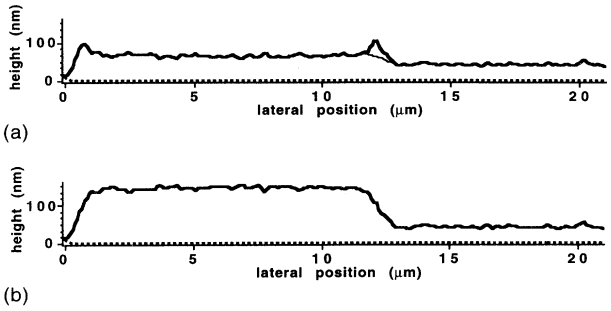

FIG. 8. Cross-sectional profiles of a spreading finger for which the upper membrane closely approaches the lower. As in Fig. 7, two forms were calculated using Eq. (2). Again, the form in (b) is possible only if the intensity maximum reaches the first peak in Fig. 1 (≈ 100 nm). Since this is often not the case, (a) with a bulging front, again seems more likely. However, in the case of close adhesion of the two bilayers, the bright peak between the dark region and the flickering region [Fig. 6, peak at right in Fig. 8(a)] may be an artifact due to scattering from the steeply bent membrane at this interface, rather than an actual reflection of the height above the surface. We have sketched in a curve (thin solid line) that seems a more likely representation.

The often jagged paths of the fjords, as well as depinning events, suggest that finger formation is often initiated and maintained by defects in the surface: a defect obstructs the forward motion, the membrane spreads on both sides of it, and a narrow seam separating two fingers originating at the defect forms. Thus, the fingers formed by vesicles spreading on MgF_2 are narrower than those on MgF_2 covered by avidin, for which the roughness of the underlying MgF_2 has been smoothed over (compare

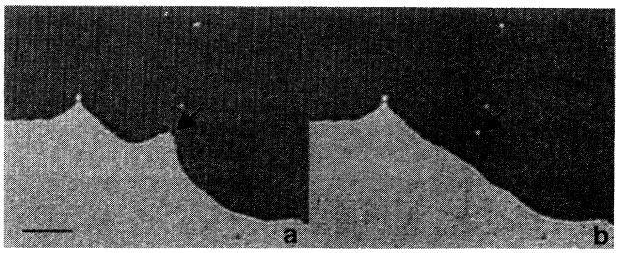

FIG. 9. Depinning event. The arrows indicate a defect on the surface. The membrane (darker region) is at first obstructed, and then comes unpinned. Another defect where the membrane remains pinned is also visible. The bar is 5 μm long.

Figs. 3 and 4). The stronger adhesion energy of MgF_2 also means that the spreading is faster, and often culminates in the vesicle bursting.

In general, two classes of fingering observations can be distinguished: one is characterized by a bulged edge contour with visible interference fringes, fluctuations of the distal membrane, and a fingerlike spreading pattern with small corrugated prewetting tips (Fig. 4). Other vesicles spread with a much broader front. These exhibit no interference fringes at the edges, and lack the small precursor tips. The shape of the contact area is, as before, determined by the surface roughness. However, very few fjords develop, and instead, the front is marked by distinct pinned points, giving it a scalloped appearance, with the membrane straining forward between the defect obstacles. Depinning events are common (Fig. 9). Since the two classes can be observed next to each other, this difference lies in the vesicles, and not in the surface roughness. The latter may be multilamellar vesicles, or, as favored by the lack of undulations, they may be vesicles with the upper bilayer already adhered to the lower.

IV. DISCUSSION

We have demonstrated that for moderately strong nonspecific solid-vesicle interactions, vesicles exhibiting large excess areas spread on the substrate without disrupting. Flat prolate vesicles with a bulged rim of fractal form exhibiting pronounced undulatory excitations (flickering) form. As has been shown in separate studies [10,11], the repulsive undulation forces of vesicles subject to slight lateral tensions are strong enough to result in a second energy minimum at a distance of about 30 ± 10 nm from the substrate; the interbilayer distance of ≈ 70 nm measured here could thus well be determined by the undulation forces. This state is, however, metastable and often the spreading lobes collapse from the center. The interbilayer thickness of the vesicle decreases from about 70 nm to 30 ± 10 nm. In the final collapsed state the distal bilayer does not flicker, and the interbilayer distance of about 30 ± 10 nm is therefore determined by the van der Waals and electrostatic interactions. The separation is larger than expected from van der Waals interactions [12], and thus points to an electrostatic repulsion the origin of which is still unclear.

In separate preliminary experiments we studied the effects of specific interactions by incorporating 10% biotin-X-DHPE (*N*-((6-(biotinoyl)amino)hexanoyl)-1,2-dihexadecanoyl-sn-glycero-3-phosphoethanolamine, triethylammonium salt; Molecular Probes, Eugene, OR) into DMPC or EggPC vesicles. These vesicles adhered strongly to surfaces coated with the ligands for biotin—avidin or streptavidin. In RICM, small stringy irregular patches of adhered membrane are observed. It appears that aggregation of biotin by lateral phase separation in the membrane occurs upon binding, causing an increase in the local membrane curvature, or possibly crystallization, and causing the large vesicles to burst and form a multitude of small ones. This is supported by our observations (not shown) of biotin-X-DPPE containing vesicles in phase contrast microscopy: upon addition of streptavidin to the solution, the large unilamellar vesicles were no longer to be found, and the sample was suddenly littered with tiny lipid debris. It should be noted that the reversible aggregation of intact vesicles under similar conditions reported by Chiruvolu *et al.* [13] was for small vesicles (50 nm diameter).

In marked contrast, nonspecific interactions induce a large adhesion contact area, and unless the attraction is strong enough to cause bursting, leaves the vesicles topologically intact. The driving force for the observed spreading is the attraction of the proximal phospholipid membrane to the surface. The fingerlike spreading of the vesicles can be rationalized in terms of two different mechanisms.

(1) Local expulsion of water through pores in the membrane at the edge causing advancement of a lobe in a stepwise fashion, with the stepsize on the order of 1 μm.

(2) Classical viscous fingering in analogy to the theory of Saffman and Taylor [14,15]. This model is presented in the Appendix.

At present we do not have a model that explains all of our observations. In the second model above, the dynamics of the spreading is determined mainly by the mutual friction between the inner and outer leaflets of the bilayer at the leading front. In the framework of this model, the less viscous fluid corresponds to the flat flickering region of the membrane and the more viscous fluid corresponds to the curved edges (cf. Fig. 10); the assumption of fluid

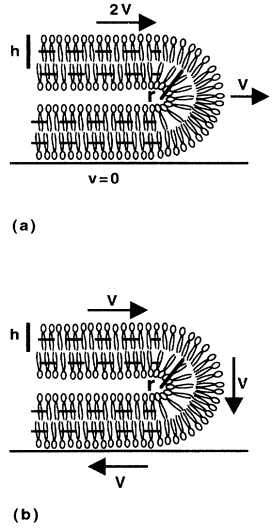

FIG. 10. Schematic presentation of simple one-dimensional spreading with a constant interbilayer separation in a laboratory system (a) and in a coordinate system moving with the edge, when the motion becomes stationary (b). r is half the distance between the centers of the bilayers and also the radius of curvature of the edge and h is the monolayer thickness. The neutral surface is defined here as the center plane of each monolayer (dashed lines), and the surface of contact is where the two monolayers meet. The viscosity of the membrane is lower in the flat region than in the curved edge region.

flow from low to high viscosity then predicts classical viscous fingering. However, since the advancement occurs in both the concave and convex regions of the edge in an uncorrelated way, we think the spreading in the present case is dominated by the former mechanism. Furthermore, in contrast to classical viscous fingering where the volume of the fluid remains constant, in the spreading observed here, the vesicle loses volume during spreading. The expulsion of water is necessary to allow further adhesion, as it makes the required excess area available. A combination of the two theories above may better explain our observations.

An intriguing aspect of the vesicle spreading is that it exhibits some striking similarities to crawling of amoeba-like cells (e.g., *Dictyostelium discoideum)* on substrates. Pseudopod formation occurs by spreading of thin lobes (~ 2 μm) on a surface. Although an actin gel forms simultaneously within these lobes, and this so-called gelation is often considered to be the driving force of pseudopod formation, it appears likely that pseudopod advancement is actually controlled by spreading of the plasma membrane bilayer on the surface. This is supported by the observation that pseudopod advancement is constant as in our experiments with vesicle spreading [16].

Many questions remain. We are continuing these investigations, with the primary goal of achieving a system in which the degree of adhesion is controllable and even reversible.

ACKNOWLEDGMENTS

This work was supported by the Deutsche Forschungsgemeinschaft (Sonderforschungsbereich 266). Further support by the Fond der Chemischen Industrie is also gratefully acknowledged. T.F. is grateful for support from the Alexander von Humboldt Stiftung, and G.W. for support from Conselho Nacional de Pesquisas (CNPq). We also wish to thank M. Peterson, J. Rädler, H. Ringsdorf, and F. Rondelez for interesting and helpful discussions, and M. Schindl for the use of his automated speed measurement program.

APPENDIX: VISCOUS FINGERING MODEL

In the following we discuss vesicle spreading in terms of the classical model of viscous fingering. We consider first a hypothetical case of spreading, where the two phospholipid bilayers are assumed to slide by each other at constant separation forming a straight front with a circular profile, and with the upper layer rolling over and adhering to the substrate (Fig. 10). The driving force for this motion is the adhesion energy of the substrate W (J/m^2). The lower bilayer is fixed by the substrate ($v=0$) and the upper one moves with a velocity $2V$, with the resulting edge velocity V.

Before considering the relevant dissipation forces that determine the resistance of the system against the driving force and consequently the velocity V, we look in more detail at the structure of the front edge and the distribution of molecules there. One can distinguish in principle two limiting cases. For very fast motion and for a slow effective diffusion, which is a consequence of the mechanically driven slip between the monolayer [16], the system does not have enough time to relax by diffusion, and the outer layer is expanded at the edge while the inner layer is compressed. In the other limit, the quasistatic case, i.e., for very slow motion and for fast diffusion, the molecules have enough time to rearrange, and one obtains equal density in the outer and inner layers of the edge, but the number of molecules in the outer layer is now larger than in the inner one. The mechanically driven diffusivity has been estimated by analyzing the microtube extrusion from macroscopic bilayer vesicles to be $D \approx 10^{-10}$ m^2/s [17]. We are interested in the case for which the interbilayer separation is small ($r < 10^{-7}$ m) and the observed velocities are also small ($V \approx 10^{-7}$ m/s). The diffusivity D divided by the length of the curved part of the edge, πr, gives, for this case, a typical "diffusion velocity" $D/\pi r > 3\times 10^{-4}$ m/s, which is more than three orders of magnitude larger than the velocity V. Therefore, we always have the quasistatic case and the density of phospholipid molecules is the same at the neutral surfaces of the external and internal monolayers.

To study the motion of the layers, it is convenient to be in a coordinate system moving with the velocity V of the edge. In such a coordinate system [Fig. 10(b)] we observe a stationary state, where the membrane moves everywhere tangentially with a constant velocity V. Since the same number of molecules enters as leaves the curved part of each monolayer, the velocities of the two monolayers at their neutral surfaces must everywhere equal V. The velocities of the two monolayers at their contact surfaces are, however, not equal. Because of the curvature, $c=1/r$, the velocity of the outer monolayer at the contact surface is $u_+ = V(1-\frac{1}{2}hc)$, and that of the inner monolayer is $u_- = V(1+\frac{1}{2}hc)$, where h is the thickness of the monolayer and the neutral surface is defined to be at the middle of the monolayer (Fig. 10). The difference is then

$$\Delta V = hcV \ , \tag{A1}$$

which leads to a friction f_e per unit length at the edge

$$f_e = \pi r b \Delta V = \pi b h V \ , \tag{A2}$$

where b is the interfacial drag coefficient [17,18] and the friction acts at the curved edge region πr.

The friction must compensate the adhesion energy W

$$W = \pi b h V \ . \tag{A3}$$

The interfacial drag coefficient for fluid bilayers has been shown to be of the order $b \approx 5\times 10^8$ N s/m^3 [17], but it can be larger if one of the monolayers is solid [$b \approx (1-5)\times 10^9$ N s/m^3] [18]. For the strongly curved surfaces in our model, the lipid tails of the inner leaflet are expanded and those of the outer leaflet are pressed together with respect to a flat bilayer. The compressed tails of the outer leaflet may therefore be expected to behave similarly to solid monolayers. We therefore take $b \approx 5\times 10^8 - 5\times 10^9$ N s/m^3. With $h = 2\times 10^{-9}$ m, and $V = 10^{-7}$ m/s a typical velocity of DMPC on avidin, we obtain for the adhesion energy $W = 3\times 10^{-7} - 3\times 10^{-6}$

J/m^2, which is, as expected, much larger than the estimated adhesion energy of DMPC on glass ($\approx 2\times 10^{-9}$ J/m^2) [19].

Another source of friction, which becomes important for longer lobes, arises from the shear motion of the two bilayers. With the relative velocity $2V$ and separation $2(r-h)$, this friction tension, distributed over the length of the membrane, is

$$f_s=\eta\frac{VL}{r-h}\ , \tag{A4}$$

where η is the viscosity of water. If both effects are taken into account, the driving tension is compensated by f_e and f_s, and the velocity V is given by

$$V=\frac{W}{\pi bh+\eta\dfrac{L}{r-h}}\ . \tag{A5}$$

The velocity is seen from this expression to be constant for short lengths L, but to slowly decrease as the effect of the shear motion of the two bilayers increases. For EggPC on avidin, with $r-h\approx 15$ nm (estimated from the measured bilayer separation cf. Fig. 6), $\eta=10^{-3}$ N s/m^2 and b as above, the crossover length $L_c=50\ \mu$m$-500\ \mu$m is obtained (cf. Fig. 4). For $L\ll L_c$ the velocity is time independent, while for $L\gg L_c$ the velocity is expected to decrease as $t^{-1/2}$. In Fig. 5 we have plotted the average velocity as a function of time for a spreading finger. The general behavior agrees with the model presented here (curve in Fig. 5). It should be noted, however, that the values in Fig. 5 are averages of several measurements, and that the motion itself is abrupt rather than smooth.

In the above analysis we have assumed a circular azimuthal cross-sectional edge profile. The profile of the edge is determined by the boundary conditions at the contact to the substrate. The curvature depends on the adhesion energy and the membrane bending stiffness [8], and on the condition that the upper bilayer eventually becomes parallel to the adhered bilayer. Such a profile has the same contributions to the friction as a circular profile [Eq. (A2)]. We have shown that the main resistance to the motion appears in the edge part of the bilayer because of the relative motion of two monolayers. Even for longer lengths L, when the relative motion of two bilayers contributes to the friction, the friction per unit length is much larger in the curved part of the membrane than elsewhere. Movement of the membrane from the flat part to the curved part can be compared to the motion of a less viscous fluid into a more viscous fluid: in the curved edge the lipids are compressed (high relative viscosity), while in the flat, undulating region the excess area indicates that the fluid is not compressed (low relative viscosity). It can therefore be expected that a straight spreading front will not be stable and a form of viscous fingering will appear. In our case, this would mean that the convex regions of the front should propagate faster. Indeed, the flow of membrane in this case spreads out and the local velocity is therefore higher in the leading edge than for a flat front. In the concave regions the opposite effect occurs, so that the growth is slower. In analogy to viscous fingering problems [15], a straight spreading front is therefore unstable. As in viscous fingering problems, it is the surface tension which stabilizes the finite size of the fingers. In our case the surface tension corresponds to the intramonolayer viscosity and the bending energy of the edge.

[1] P. G. de Gennes, Rev. Mod. Phys. **57**, 827 (1985).
[2] F. Brochard-Wyart, P. Martin, and C. Redon, Langmuir **9**, 3682 (1993).
[3] L. Leger and J. F. Joanny, Rep. Prog. Phys. **55**, 431 (1992).
[4] D. K. Schwartz, R. Viswanathan, and J. A. N. Zasadzinski, J. Phys. Chem. **96**, 10 444 (1992).
[5] S. M. Troian, E. Herbolzheimer, and S. A. Safran, Phys. Rev. Lett. **65**, 333 (1990).
[6] G. Elender and E. Sackmann, J. Phys. (France) II **4**, 455 (1994).
[7] M. Schindl *et al.* (unpublished).
[8] U. Seifert and R. Lipowsky, Phys. Rev. A **42**, 4768 (1990).
[9] M. I. Angelova and D. S. Dimitrov, Mol. Cryst. Liq. Cryst. **152**, 89 (1987).
[10] J. Rädler and E. Sackmann, J. Phys. (France) II **3**, 727 (1993).
[11] J. O. Rädler, T. J. Feder, H. Strey, and E. Sackmann (unpublished).
[12] W. Frey and E. Sackmann (unpublished).
[13] S. Chiruvolu *et al.*, Science **264**, 1753 (1994).
[14] P. G. Saffman and G. I. Taylor, Proc. R. Soc. London Ser. A **245**, 312 (1958).
[15] D. A. Kessler, J. Koplik, and H. Levine, Adv. Phys. **37**, 255 (1988).
[16] E. Sackmann, J. Rädler, and M. Schindl (unpublished).
[17] E. Evans, A. Yenny, R. Wangh, and S. Sung, in *The Structure and Conformation of Amphiphilic Membranes*, Springer Proceedings in Physics Vol. 66, edited by R. Lipowsky, D. Richter, and K. Kremer (Springer-Verlag, New York, 1992).
[18] R. Merkel, E. Sackmann, and E. Evans, J. Phys. (France) **50**, 1535 (1989).
[19] J. Rädler, Ph.D. thesis, Technische Universität München, 1993.

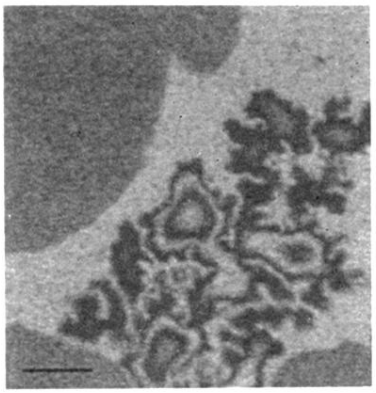

FIG. 3. DMPC vesicles were introduced to a bare MgF_2 surface. Most vesicles burst, forming large regular patches, from which the bilayer thickness can be determined. The central region of this figure shows fingering of closed vesicles on the same surface. The scale of fingers is smaller than on avidin (Fig. 4). The bar is 5 μm long.

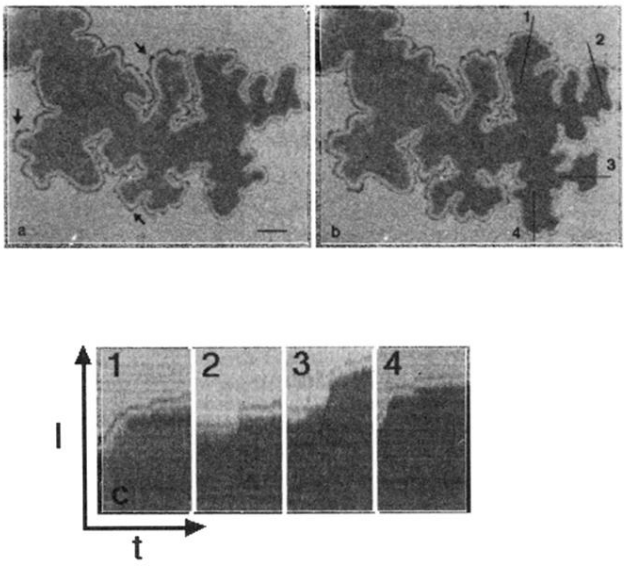

FIG. 4. EggPC vesicle spreading on an avidin surface. (a) and (b) are the first and last images in a 64 image sequence, 36 s apart. The higher intensity in the upper left corner is due to reflections from the clump, located just outside the field of view. (c) shows the advancement of the front of the fingers in the directions marked in (b). Each speed profile is a composite of the intensity profiles for the 64 frame sequence, with time proceeding to the right (t), and the position of the moving front plotted on the vertical axis (l). The average speed is then obtained from the slope (the speeds during the fast spurts, as opposed to the average overall speed, are given in parentheses): 1: 90 nm/s (310 nm/s); 2: 40 nm/s (720 nm/s); 3: 110 nm/s (850 nm/s); 4: 70 nm/s (390 nm/s). (a) and (b) are reduced in size relative to (c). The bar is 5 μm long.

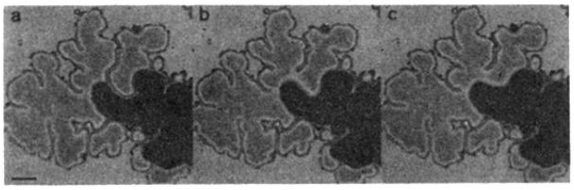

FIG. 6. EggPC vesicle spreading on avidin surface. The dark regions in this figure indicate the adhesion of the upper membrane to the lower, already adhered one. This adhesion mostly follows the existing fjords, but sometimes induces the disappearance of one, as seen in this series of images (arrow) ($\Delta t_{AB} = 0.08$ s, $\Delta t_{BC} = 1.8$ s). The bar is 5 μm long.

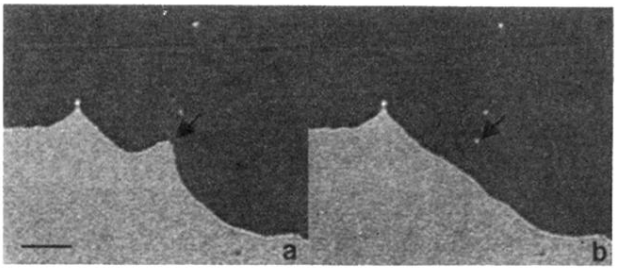

FIG. 9. Depinning event. The arrows indicate a defect on the surface. The membrane (darker region) is at first obstructed, and then comes unpinned. Another defect where the membrane remains pinned is also visible. The bar is 5 μm long.